Chemical Physics Letters 804 (2022) 139889

Contents lists available at ScienceDirect

Chemical Physics Letters

journal homepage: www.elsevier.com/locate/cplett

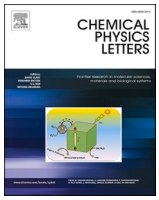

In situ XAFS study of the chemical state of a Co catalyst during single-walled carbon nanotube growth under conventional growth conditions using alcohol catalytic chemical vapor deposition

Shusaku Karasawa [a], Kamal Prasad Sharma [b], Daiki Yamamoto [a], Takahiro Saida [a,b], Shigeya Naritsuka [c], Takahiro Maruyama [a,b,*]

[a] Department of Applied Chemistry, Meijo University, Nagoya 468-8502, Japan
[b] Nanomaterial Research Center, Meijo University, Nagoya 468-8502, Japan
[c] Department of Materials Science and Engineering, Meijo University, Nagoya 468-8502, Japan

ARTICLE INFO

Keywords:
Carbon nanotube
XAFS
Raman
Catalyst
Co

ABSTRACT

In situ X-ray absorption fine structure spectroscopy (XAFS) analysis was performed on cobalt (Co) catalysts during single-walled carbon nanotube (SWCNT) growth by alcohol catalytic chemical vapor deposition. Co K-edge XAFS analysis showed that Co catalysts prepared from Co acetates were composed of both Co oxides and carbides, which were reduced as the temperature increased to 800 °C. Upon addition of ethanol, the Co catalysts gradually changed to carbides. Our results show that Co catalysts are mainly composed of carbides formed during SWCNT growth under conventional growth conditions in alcohol catalytic chemical vapor deposition (ACCVD).

1. Introduction

Single-walled carbon nanotubes (SWCNTs) [1] are tubes made of carbon with diameters typically measured in nanometers with interesting properties such as high carrier mobility [2], large current density [3], and high specific surface area [4]. Additionally, they can behave as both semiconductors and metals, depending on their chirality [5]. Therefore, SWCNTs have potential use in electronics applications. Owing to the electronic structure of an SWCNT depending on its chirality, selective growth of SWCNTs with unique chirality is sought after and heavily researched. Currently, chemical vapor deposition (CVD) is widely used for SWCNT growth as it can be used for mass production and is cost-effective [6]. During CVD, nanosized metal particles react with the feedstock gas at high temperatures (typically 700–1000 °C) to produce SWCNTs. Consequently, the size, structure, and chemical state of the catalyst particles influence the diameter and chirality of the SWCNTs. Therefore, it is useful to elucidate the chemical states of catalyst particles during SWCNT growth.

To date, various experimental techniques, such as transmission electron microscopy (TEM) [7,8], atomic force microscopy (AFM) [9,10], X-ray photoelectron spectroscopy (XPS) [11,12], and X-ray diffraction (XRD) [11,13], have been utilized to investigate the catalyst particles used for SWCNT growth. However, most of the analyses were performed after SWCNT growth was terminated, and the "real" states of the catalyst particles during SWCNT growth are not fully understood. Recently, *in situ* analysis techniques have been developed to probe the physical and chemical states of catalyst particles during SWCNT growth, e.g., environmental TEM (ETEM) for Fe [14], Co [15–19], and Ni [20] catalysts, where CO, CH_4, C_2H_2, and C_2H_4 were used as feedstock gases. However, most of these ETEM observations were performed below 700 °C, although typical temperatures during the conventional CVD growth of SWCNTs were in the range of 700–1000 °C. This could be attributed to the limitations of TEM, where an electron beam was used as the probe. Furthermore, although alcohol catalytic CVD (ACCVD) is one of the most common techniques for growing SWCNTs [21–23], to our knowledge, *in situ* analysis of catalysts during SWCNT growth, using ethanol as the feedstock, has never been reported.

In this study, we utilized X-ray absorption fine structure (XAFS) analysis to investigate the chemical states of the catalyst particles during SWCNT growth via ACCVD. XAFS is a powerful method that has been broadly applied for *in situ* material characterization under a wide range of conditions [24,25]. XAFS analysis can be performed at both high temperatures [26] and pressures [27]. Therefore, it can be used for the *in situ* analysis of catalyst particles during SWCNT growth under

* Corresponding author at: Department of Applied Chemistry, Meijo University, Nagoya 468-8502, Japan.
E-mail address: takamaru@meijo-u.ac.jp (T. Maruyama).

https://doi.org/10.1016/j.cplett.2022.139889
Received 19 May 2022; Received in revised form 9 July 2022; Accepted 19 July 2022
Available online 21 July 2022

conventional CVD growth conditions (700–800 °C, 10–10^5 Pa). Additionally, the measurement of fine structures near the absorption edges (X-ray absorption near edge structure (XANES)) provides chemical fingerprints that can be used to identify specific phases, including the valence states of target elements. Analysis of the fine structure far above the edge – the extended X-ray absorption fine structure spectroscopy (EXAFS) region – provides structural information owing to the contributions of local photoelectron scattering [28–31]. We performed XAFS analysis for both the XANES and EXAFS regions to investigate the chemical states of the Co catalyst during SWCNT growth at 800 °C under an ethanol gas supply. The variation in the chemical composition of the Co catalyst particles during temperature rise, SWCNT growth, and cooling was determined.

2. Experimental procedure

2.1. Sample preparation

Co(II) acetate was stirred in deionized (D.I.) water using a mixer for 15 s; the concentration of Co in D.I. water was 0.10 M. Subsequently, both BN nanoslurry (BN average particle size ~50 nm, MARUKA, SL-170-20-OG) and BN microparticles (BN particle size 55–60 μm, Kojundo Chemical Laboratory Co. Ltd., BB103PB) were added to the aqueous solution containing Co ions, and the mixture was stirred for 15 s, followed by sintering at 500 °C for 10 min to dehydrate the sample. The dehydrated samples were ground to a powder form and molded into disk-shaped pellets (thickness of ~1 mm) using a tablet-mold machine. The obtained CoBN pellets consisted of Co nanoparticles formed on BN particles.

2.2. XAFS analysis

The *in situ* analysis to obtain Co K-edge XAFS spectra was performed at the BL-11S2 beamline of the Aichi SR (Japan) in transmission mode. The CoBN pellet was placed inside a CVD reactor at the beamline, which was designed for *in situ* XAFS measurements. Schematics of the setup are shown in Fig. 1 (a), and the time sequences of the temperature and gas flow are summarized in Fig. 1 (b). After evacuating the CVD reactor to a pressure below 2 Pa using a scroll pump, Ar carrier gas was introduced into the reactor at a flow rate of 1000 sccm. The temperature of the sample was then increased to 800 °C at a rate of 13 °C/min. After the temperature reached 800 °C, ethanol gas was supplied to the reactor at a rate of 25 sccm to grow SWCNTs with Ar carrier gas. The pressure in the furnace was maintained at ~360 Pa and the temperature was maintained at 800 °C for 10 min during SWCNT growth. Subsequently, the ethanol supply was stopped, and the sample was allowed to cool to room temperature at a rate of approximately 13 °C/min.

XAFS measurements using the quick XAFS (QXAFS) mode were performed during the temperature increase, SWCNT growth, and cooling stages. One minute was required to obtain one spectrum using the QXAFS. The obtained XAFS spectra were analyzed using the Athena software, a program for analyzing XAFS data. Data reduction of the XAFS spectra involved energy calibration, background subtraction, and normalization. Subsequently, the EXAFS region of the XAFS spectra were processed using Athena software. After background removal and normalization, the spectra were converted to *k*-space and the background was subtracted in *k*-space using a cubic spline fit. Subsequently, the spectra were truncated within a range of 3–10 Å. To obtain the radial structure function (RSF), a Fourier transform was performed on the spectra in k-space using a Hanning window function; a k-weighting of 3 was employed to emphasize scattering by the light atoms. The first-coordination shells were fitted in the *k*-range of 3–10 Å.

2.3. Characterization of SWCNT

After performing *in situ* XAFS measurements, the CoBN pellets were characterized by Raman spectroscopy (Raman; RAMANforce, Nanophoton, Osaka, Japan) and transmission electron microscopy TEM (HF-2000, Hitachi, Tokyo, Japan). Raman spectroscopy measurements were performed at an excitation wavelength of 671 nm. The surface of the pellet was scratched and dropped onto a TEM grid for TEM observation, which was performed using an acceleration voltage of 200 kV.

3. Results and discussion

3.1. In situ XAFS analysis during temperature rise

Fig. 2 (a) shows the Co K-edge X-ray absorption near edge structure (XANES) region of the XAFS spectrum of the as-prepared sample. The red solid line corresponds to the sample obtained immediately after being molded into a disk-shaped pellet. For comparison, the XAFS spectra of Co and the various Co compounds are shown with dotted lines. The XAFS spectrum of the as-prepared sample exhibits a sharp absorption peak at 7724.7 eV and pre-edge peak at approximately 7712 eV is quite weak, indicating the oxidation of Co particles [29]. However, the absorption peak energy for the as-prepared Co catalysts was slightly lower than that of CoO (7726.3 eV), suggesting that the as-prepared Co catalysts were not entirely composed of CoO, but also included various oxides containing carbon atoms. To characterize the as-prepared sample in more detail, we calculated the RSF of the as-prepared Co catalyst, as shown in Fig. 2(b), which was obtained from the XAFS spectrum in the EXAFS region. As a reference, the bond length regions of Co-Co, Co-C, and Co-O are also shown, which were determined from previous EXAFS results on metallic Co, Co_3C, and Co_3O_4 [19,32]. In Fig. 2(b), a distinct peak was seen at the distance, corresponding to the bond length regions of Co-O. This confirms that the as-prepared Co nanoparticles were mainly composed of Co oxides and that the amount of metallic Co was negligible.

When the temperature was increased to 800 °C using only the carrier gas, *in situ* Co K-edge XAFS measurements were performed for the Co catalysts. Fig. 3 (a) shows the Co K-edge XANES spectra with increasing temperature. A sharp peak was observed at the absorption edge of

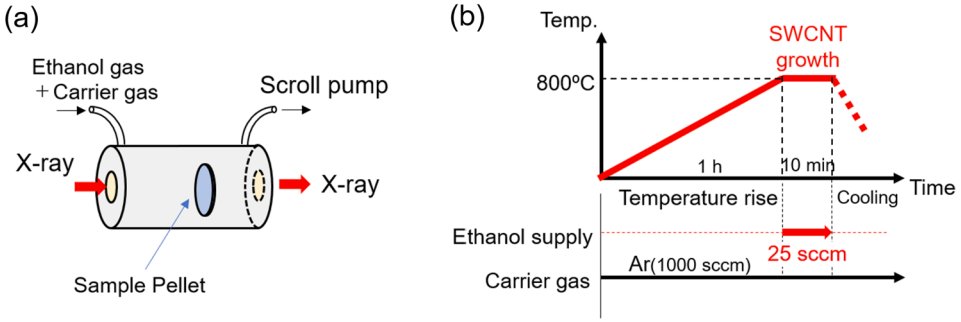

Fig. 1. (a) Schematics of the CVD reactor and its setup used for *in situ* XAFS. (b) Time sequences of temperature and gas flow during *in situ* XAFS analysis.

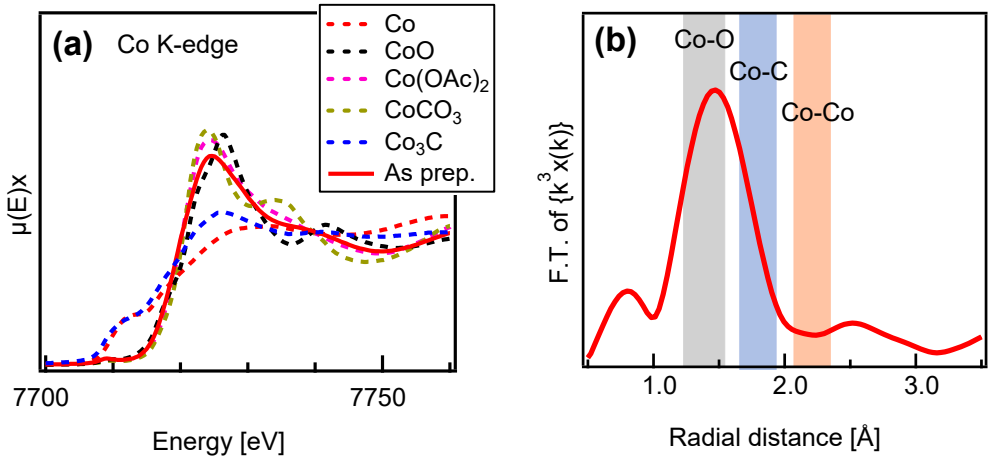

Fig. 2. (a) Co K-edge XANES spectrum of as-prepared Co catalysts from Co(II) acetate (red solid line). For comparison, XANES spectra of Co metal, CoO, $Co(OAc)_2$, $CoCO_3$, and Co_3C are shown as dotted lines. (b) Fourier transforms of the Co K-edge EXAFS spectra of as-prepared Co catalysts. As reference, the bond length regions of Co-Co, Co-C, and Co-O were also shown, which were determined from previous EXAFS results on metal Co, Co_3C, and Co_3O_4 [19,32].

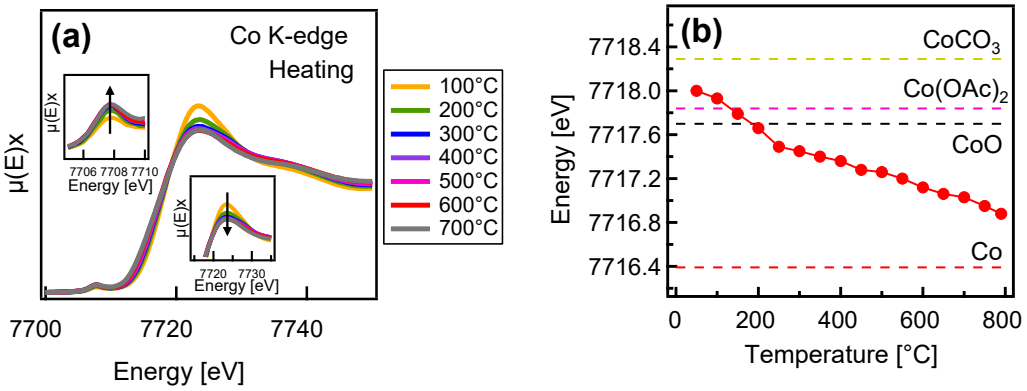

Fig. 3. (a) *In situ* Co K-edge XANES spectrum during temperature rise. The insets show magnified spectra in the pre-edge and white line regions. (b) Temperature dependence of of Co K-edge shifts measured at half the step height in the spectra. Edge shifts for $CoCO_3$, $Co(OAc)_2$, CoO, and metal Co are shown for comparison.

7724.1 eV for the as-prepared sample (Fig. 2 (a)). However, with the increase in temperature, the intensity of the first intensive peak after the absorption edge (white line) decreased, while the intensity of the pre-edge peak at 7707.7 increased, as shown in the insets of Fig. 3 (a). This suggests that the Co catalysts were reduced as the temperature increased.

To clarify the differences in the energy shift, the energy at a half-step height (where the normalized absorbance is 0.5) at the absorption edge was calculated for each spectrum. It is generally considered that this value can be used to estimate the average oxidation state. The variation

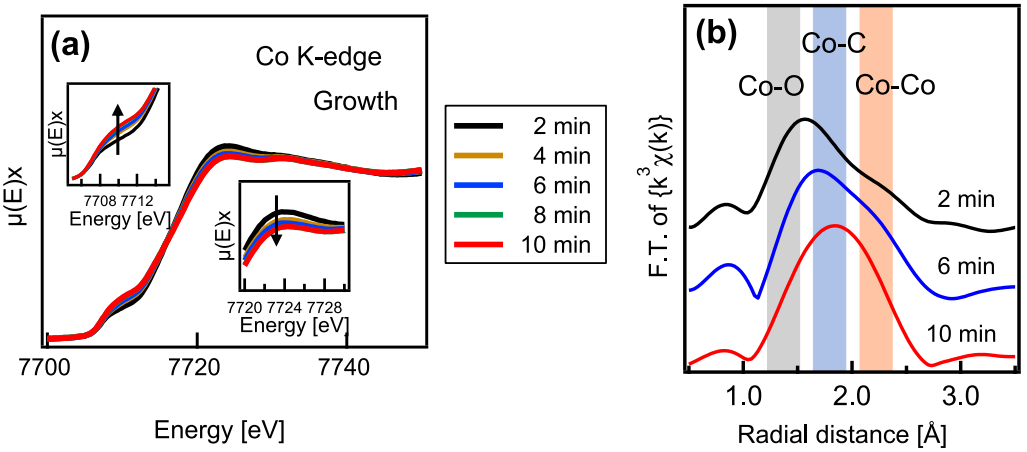

Fig. 4. (a) *In situ* Co K-edge XANES spectra during SWCNT growth. The insets show magnified spectra in the pre-edge and white line regions. (b) Fourier transforms of the Co K-edge EXAFS spectra after SWCNT growth for 2, 6 and 10 min. As reference, the bond length regions of Co-Co, Co-C, and Co-O are also shown, which are determined from previous EXAFS results on metal Co, Co_3C, and Co_3O_4 [19,32].

in energy at the half-step height of the Co K-edge XAFS spectra during the temperature rise is shown in Fig. 3 (b), where the energies at half-step heights of $CoCO_3$, Co acetate, CoO, and metal Co are also shown. Before heating started, the energy at the half-step height was 7718.0 eV, which gradually shifted to 7716.8 eV when the temperature reached 800 °C. This confirmed that the reduction of the Co catalysts proceeded as the temperature increased. However, the energy at the half-step height at 800 °C was higher than that of metallic Co, suggesting that the Co catalysts were not completely reduced to metallic Co, but also included Co oxides and carbides at the start of SWCNT growth.

3.2. *In situ* XAFS analysis during SWCNT growth and cooling

We also performed *in situ* XAFS measurements during SWCNT growth at 800 °C with ethanol supply, and during the cooling stage to room temperature after stopping the ethanol supply. Fig. 4 (a) shows the Co K-edge XANES spectra during SWCNT growth. As the growth time increased, the intensity of the absorption edge at approximately 7724 eV decreased, while the intensity of the pre-edge peak at approximately 7710 eV increased, as shown in the insets of Fig. 4 (a). This suggests that the composition of the Co catalysts varied during the SWCNT growth. To investigate the variation in the bonding of Co with the surrounding atoms, we obtained the RSFs from the FT of the EXAFS. Fig. 4 (b) shows the RSFs for the sample after SWCNT growth for 2, 6, and 10 min, which were obtained from the *in situ* XAFS spectra during SWCNT growth. As a reference, the bond length regions of Co-Co, Co-C, and Co-O are also shown [19,32]. After SWCNT growth for 2 min, a main peak was observed at around 1.5 Å in the first nearest neighbor, and a shoulder peak was seen at around 2.3 Å, corresponding to Co-Co bonding. This suggests that the Co catalysts were not only metallic Co, but also Co compounds containing oxides and carbides soon after the SWCNT growth started. As the growth time increased, the main peak in the first nearest neighbor shifted to ~1.8 Å, corresponding to Co-C bonding, while the intensity of the shoulder peak decreased. This suggests that the Co catalysts gradually became carbides during SWCNT growth, although there is a possibility that a small amount of metallic Co and Co oxides were present in the Co catalyst during SWCNT growth, considering the full width at half maximum of the main peak for the growth time of 6 min. Generally, not all catalyst particles act as active in SWCNT growth, and it would be true in our experiment. Nevertheless, considering that the composition of Co carbide became dominant during SWCNT growth, active catalysts would be Co carbide, even though the composition of inactive ones were included in XAFS spectra.

After the ethanol supply was stopped, heating of the furnace was stopped and the sample was gradually cooled to room temperature. In addition, we performed *in situ* XAFS measurements during this cooling duration. The temperature dependence of the XANES region is shown in Fig. 5 (a) and the RSFs obtained from the EXAFS region are shown in Fig. 5 (b). After the ethanol supply was stopped, the XAFS spectra in the XANES region underwent very little change; however, with a decrease in temperature, the main peak in the RSFs, which were estimated from the XAFS spectra in the EXAFS region, shifted to longer distances. This suggests that the Co catalysts were reduced towards metallic Co as the temperature decreased. Below 300 °C, the main peak was at approximately 2.2 Å, indicating that the Co catalysts were mainly composed of metallic Co. These results during SWCNT growth and cooling imply that *in situ* analysis is essential for determining the chemical states of the catalyst particles during SWCNT growth.

3.3. Characterization of SWCNTs

To confirm SWCNT growth during *in situ* XAFS analysis, Raman spectroscopy and TEM observations were performed. Fig. 6 (a) and (b) show the Raman spectra of the sample after *in situ* XAFS analysis, where the Raman spectra in the low- and high-frequency regions are shown separately. To perform the Raman measurements, the surface of the CoBN pellet was scratched onto Si substrates using a razor blade. Therefore, a Si-derived phonon peak was observed at 302 cm^{-1} in the radial breathing mode (RBM) region of the Raman spectrum. An RBM peak was observed at 227.6 cm^{-1}, as indicated by the arrow in Fig. 6 (a). The G band peak appeared in the high-frequency region (Fig. 6 (b)) and was split into G^- and G^+ bands. This result confirms the growth of SWCNTs during *in situ* XAFS analysis. The TEM image shows that SWCNTs with a diameter of approximately 1 nm were present, as indicated by the white arrows, further confirming the growth of SWCNTs.

3.4. Growth process of SWCNTs from a catalyst particle

We found that Co catalysts prepared using Co acetates were not completely reduced to metallic Co upon heating at 800 °C under a flow of Ar, which would be composed of Co oxides containing carbon atoms. However, during SWCNT growth in the presence of ethanol gas, the Co catalysts were carbonized to form Co carbides. Previously, *in situ* analyses of Co nanoparticles during SWCNT growth were performed via ETEM observations at 600–750 °C using CO, CH_4, C_2H_2, and C_2H_4 as feedstock gases [15–19] (Table 1). Apart from ETEM analysis by He et al. [15], the Co nanoparticles were carbonized during SWCNT growth. In Ref. [15], they performed SWCNT growth at 600 °C and concluded that

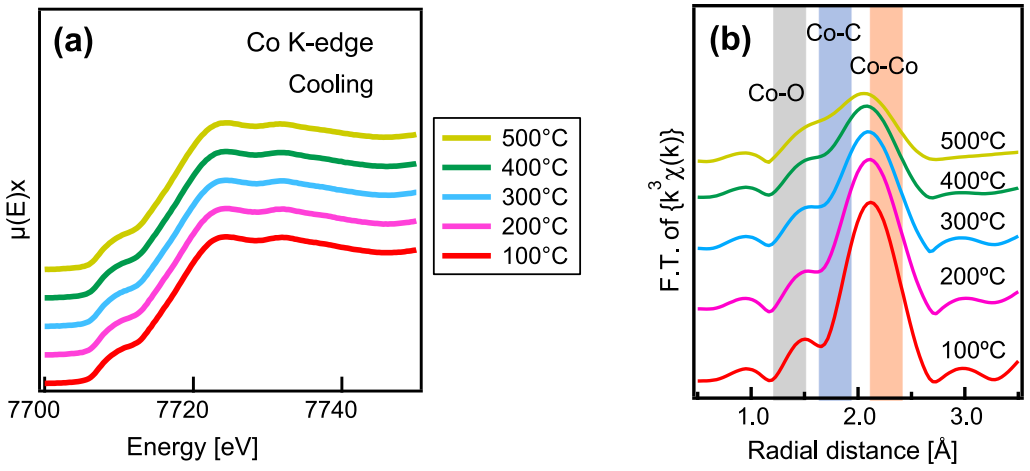

Fig. 5. (a) *In situ* Co K-edge XANES spectra during cooling. (b) Fourier transforms of the Co K-edge EXAFS spectra at 100, 200, 300, 400, and 500 °C during cooling. As reference, the bond length regions of Co-Co, Co-C, and Co-O are also shown, which are determined from previous EXAFS results on metal Co, Co_3C, and Co_3O_4 [19,32].

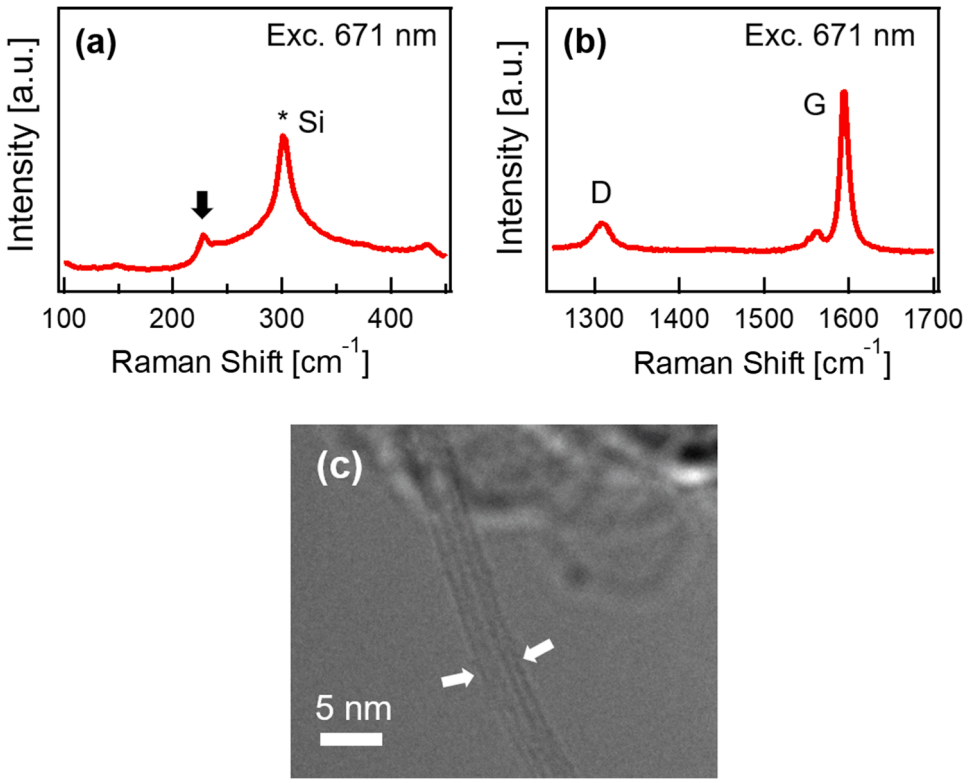

Fig. 6. Raman spectra in (a) the RBM region and (b) the high frequency region of the sample after *in situ* XAFS analysis. The excitation wavelength was 671 nm. (c) TEM image for grown SWCNTs after *in situ* XAFS analysis.

Table 1
Previous studies on chemical states of catalysts during SWCNT growth by ETEM.

Catalyst	Carbon source	Temp.	Pressure	Chemical state during SWCNT growth	Ref.
Co	CO	600 °C	630 Pa	metal Co	[15]
Co	C_2H_2	625 °C	5.0 × 10^{-3} Pa	Co_2C, Co_3C	[16]
Co	CO	700 °C	760 Pa	Co_2C, Co_3C	[17]
Co	C_2H_2	650 °C	0.01 Pa	Co, Co_2C	[18]
Co	CH_4 or CO	600–750 °C	28–503 Pa	Co, Co_3C	[19]
Fe	C_2H_2	600 °C	10 Pa	Fe_3C	[14]
Ni	C_2H_2	650 °C	5.3 × 10^{-4} Pa	Ni	[20]
Co	C_2H_5OH	800 °C	360 Pa	Co carbide	This study

metallic Co was an active catalyst. However, the growth temperature, 600 °C, was relatively low, compared to the conventional growth condition. Furthermore, the diameter of grown SWCNTs were ~5 nm and much larger than those reported in previous *in situ* analysis. Such an exceptional circumstance might lead to the contradictory result to those reported by other groups.

In Table 1, except for the SWCNT growth with CO feedstock, the ETEM observations were performed under low pressure (<0.01 Pa), and the growth temperatures were lower than those in conventional CVD. Recently, Yang et al. performed *in situ* XAFS analysis of Co nanoparticles at 700 °C, under CH_4/He supply at a flow rate of 20 sccm [19]. They found that the Co-C bond was formed under CH_4 supply, but SWCNT growth was not confirmed by Raman spectra or TEM after XAFS analysis. Additionally, *in situ* analysis of SWCNT growth by ACCVD has not yet been reported, although ACCVD is a common technique for SWCNT growth. Unlike previous *in situ* analyses, we performed *in situ* XAFS analysis under conventional growth conditions of SWCNTs by ACCVD, where the growth temperature and ethanol flow rate were 800 °C and 25 sccm (360 Pa), respectively. Combined with Raman analysis after SWCNT growth, our results showed that the Co catalyst particles were carbonized during SWCNT growth, even by ACCVD. Although the growth condition would affect the chemical states of Co catalyst particles, our results demonstrated that Co catalysts become carbides during SWCNT growth under the conventional growth condition, irrespective of the feedstock gas, owing to the tendency towards carbide formation of Co particles. This has been predicted in a simulation using the self-consistent-charge density-functional tight-binding (SCC-DFTB) method [33].

4. Conclusion

We performed *in situ* XAFS analysis during SWCNT growth under the conventional growth conditions of ACCVD (800 °C under an ethanol gas flow of 25 sccm using Ar as the carrier gas). *In situ* XAFS analysis during the temperature rise to the growth temperature under Ar gas supply showed that Co catalysts prepared by the solution method from Co acetates were gradually reduced, but Co catalysts were not completely reduced to metallic Co, even after heating to 800 °C. After the ethanol supply started for SWCNT growth, the Co catalysts gradually transformed into carbides. However, they transformed to metallic Co during cooling. We demonstrated the variation in the chemical states of the Co catalysts during SWCNT growth under the conventional ACCVD conditions using *in situ* XAFS measurements. Our results provide a collective view of the growth process of SWCNTs from catalyst particles. In addition, the usefulness of XAFS for *in situ* analysis under conventional growth conditions was demonstrated.

CRediT authorship contribution statement

Shusaku Karasawa: Conceptualization, Methodology, Data curation, Investigation, Writing – original draft. **Kamal Prasad Sharma:**

Investigation. **Daiki Yamamoto:** Investigation. **Takahiro Saida:** Investigation, Methodology. **Shigeya Naritsuka:** Investigation, Methodology. **Takahiro Maruyama:** Conceptualization, Supervision, Writing – review & editing.

Declaration of Competing Interest

The authors declare that they have no known competing financial interests or personal relationships that could have appeared to influence the work reported in this paper.

Acknowledgements

This work was partially supported by JSPS KAKENHI (Grant Number 19H02563) and the Meijo University Research Branding Project for Cultivation and Invention of New Nanomaterials under the Ministry of Education, Culture, Sports, Science and Technology (MEXT) Private University Research Branding Project (Global Development Category). Part of this work was conducted at the Institute for Molecular Science (IMS) and Nagoya Institute of Technology, supported by the Nanotechnology Platform" of MEXT. We thank Prof. Hihara at the Nagoya Institute of Technology for performing the TEM observations.

References

[1] S. Iijima, T. Ichihashi, Single-shell carbon nanotubes of 1-nm diameter, Nature 363 (6430) (1993) 603–605, https://doi.org/10.1038/363603a0.
[2] A. Javey, J. Guo, Q. Wang, M. Lundstrom, H. Dai, Ballistic carbon nanotube field-effect transistors, Nature 424 (6949) (2003) 654–657, https://doi.org/10.1038/nature01797.
[3] S. Hong, S. Myung, A flexible approach to mobility, Nat. Nanotechnol. 2 (4) (2007) 207–208, https://doi.org/10.1038/nnano.2007.89.
[4] A. Peigney, C.h. Laurent, E. Flahaut, R.R. Bacsa, A. Rousset, Specific surface area of carbon nanotubes and bundles of carbon nanotubes, Carbon 39 (4) (2001) 507–514, https://doi.org/10.1016/S0008-6223(00)00155-X.
[5] R. Saito, G. Dresselhaus, M.S. Dresselhaus, Physical Properties of Carbon Nanotubes, Imperial College Press, London, 1998, p. 59.
[6] M. Kumar, Y. Ando, Nanosci. Nanotechnol. 10 (2010) 3739, https://doi.org/10.1166/jnn.2010.2939.
[7] G.-H. Jeong, S. Suzuki, Y. Kobayashi, A. Yamazaki, H. Yoshimura, Y. Homma, Effect of nanoparticle density on narrow diameter distribution of carbon nanotubes and particle evolution during chemical vapor deposition growth, J. Appl. Phys. 98 (12) (2005) 124311, https://doi.org/10.1063/1.2146054.
[8] S. Forel, A. Castan, H. Amara, I. Florea, F. Fossard, L. Catala, C. Bichara, T. Mallah, V. Huc, A. Loiseau, C.-S. Cojocaru, Tuning bimetallic catalysts for a selective growth of SWCNTs, Nanoscale 11 (9) (2019) 4091–4100.
[9] M. Cantoro, S. Hofmann, S. Pisana, V. Scardaci, A. Parvez, C. Ducati, A.C. Ferrari, A.M. Blackburn, K.-Y. Wang, J. Robertson, Catalytic Chemical Vapor Deposition of Single-Wall Carbon Nanotubes at Low Temperatures, Nano Lett. 6 (6) (2006) 1107–1112, https://doi.org/10.1021/nl060068y.
[10] P.B. Amama, C.L. Pint, L. McJilton, S.M. Kim, E.A. Stach, P.T. Murray, R.H. Hauge, B. Maruyama, Role of Water in Super Growth of Single-Walled Carbon Nanotube Carpets, Nano Lett. 9 (1) (2009) 44–49, https://doi.org/10.1021/nl801876h.
[11] A. Castan, S. Forel, L. Catala, I. Florea, F. Fossard, F. Bouanis, A. Andrieux-Ledier, S. Mazerat, T. Mallah, V. Huc, A. Loiseau, C.S. Cojocaru, New method for the growth of single-walled carbon nanotubes from bimetallic nanoalloy catalysts based on Prussian blue analog precursors, Carbon 123 (2017) 583–592, https://doi.org/10.1016/j.carbon.2017.07.058.
[12] G. Eres, A.A. Kinkhabwala, H. Cui, D.B. Geohegan, A.A. Puretzky, D.H. Lowndes, Molecular Beam-Controlled Nucleation and Growth of Vertically Aligned Single-Wall Carbon Nanotube Arrays, J. Phys. Chem. B 109 (35) (2005) 16684–16694, https://doi.org/10.1021/jp051531i.
[13] S. Esconjauregui, C.M. Whelan, K. Maex, The reasons why metals catalyze the nucleation and growth of carbon nanotubes and other carbon nanomorphologies, Carbon 47 (3) (2009) 659–669, https://doi.org/10.1016/j.carbon.2008.10.047.
[14] H. Yoshida, S. Takeda, T. Uchiyama, H. Kohno, Y. Homma, Atomic-Scale In-situ Observation of Carbon Nanotube Growth from Solid State Iron Carbide Nanoparticles, Nano Lett. 8 (7) (2008) 2082–2086, https://doi.org/10.1021/nl080452q.
[15] M. He, H. Jiang, B. Liu, P.V. Fedotov, A.I. Chernov, E.D. Obraztsova, F. Cavalca, J. B. Wagner, T.W. Hansen, I.V. Anoshikin, E.A. Obraztsava, A.V. Belkin, E. Sairanen, A.G. Nasibulin, J. Lehtonen, E.I. Kauppinen, Chiral-Selective Growth of Single-Walled Carbon Nanotubes on Lattice-Mismatched Epitaxial Cobalt Nanoparticles, Sci. Rep. 3 (2013) 1460, https://doi.org/10.1038/srep01460.
[16] M. Picher, P.A. Lin, J.L. Gomez-Ballesteros, P.B. Balbuena, R. Sharma, Nucleation of Graphene and Its Conversion to Single-Walled Carbon Nanotubes, Nano Lett. 14 (11) (2014) 6104–6108, https://doi.org/10.1021/nl501977b.
[17] L. Zhang, M. He, T.W. Hansen, J. Kling, H. Jiang, E.I. Kauppinen, A. Loiseau, J. B. Wagner, Growth Termination and Multiple Nucleation of Single-Wall Carbon Nanotubes Evidenced by *in Situ* Transmission Electron Microscopy, ACS Nano 11 (2017) 4483, https://doi.org/10.1021/acsnano.6b05941.
[18] P.A. Lin, J.L. Gomez-Ballesteros, J.C. Burgos, P.B. Balbuena, B. Natarajan, R. Sharma, Direct evidence of atomic-scale structural fluctuations in catalyst nanoparticles, J. Catal. 349 (2017) 149–155, https://doi.org/10.1016/j.jcat.2017.03.009.
[19] F. Yang, H. Zhao, W. Wang, Q. Liu, X. Liu, Y. Hu, X. Zhang, S. Zhu, D. He, Y. Xu, J. He, R. Wang, Y. Li, Carbon-Involved Near-Surface Evolution of Cobalt Nanocatalysts: An in Situ Study, CCS Chem. 3 (2021) 154. https://doi.org/10.31635/ccschem.020.202000595.
[20] M. Lin, J.P.Y. Tan, C. Boothroyd, K.P. Loh, E.S. Tok, Y.L. Foo, Direct observation of Single-Walled Carbon Nanotube Growth at the atomic scale, Nano Lett. 6 (2006) 449, https://doi.org/10.1021/nl052356k.
[21] S. Maruyama, R. Kojima, Y. Miyauchi, S. Chiashi, M. Kohno, Low-temperature synthesis of high-purity single-walled carbon nanotubes from alcohol, Chem. Phys. Lett. 360 (3-4) (2002) 229–234, https://doi.org/10.1016/S0009-2614(02)00838-2.
[22] T. Maruyama, H. Kondo, R. Ghosh, A. Kozawa, S. Naritsuka, Y. Iizumi, T. Okazaki, S. Iijima, Single-walled carbon nanotube synthesis using Pt catalysts under low ethanol pressure via cold-wall chemical vapor deposition in high vacuum, Carbon 96 (2016) 6–13.
[23] T. Maruyama, A. Kozawa, T. Saida, S. Naritsuka, S. Iijima, Low temperature growth of single-walled carbon nanotubes from Rh catalysts, Carbon 116 (2017) 128–132, https://doi.org/10.1016/j.carbon.2017.01.098.
[24] H. Topsøe, Developments in operand studies and in situ characterization of heterogeneous catalysts, J. Catal. 216 (2003) 155, https://doi.org/10.1016/S0021-9517(02)00133-1.
[25] J. Timoshenko, B. Roldan Cuenya, In situ/operando electrocatalyst characterization by X-ray absorption spectroscopy, Chem. Rev. 121 (2) (2021) 882–961, https://doi.org/10.1021/acs.chemrev.0c00396.
[26] T. Maruyama, S. Naritsuka, K. Amemiya, In situ High-Temperature NEXAFS Study on Carbon Nanotube and Graphene Foramation by Thermal Decomposition of SiC, J. Phys. Chem. C 119 (2015) 26698, https://doi.org/10.1021/acs.jpcc.5b05854.
[27] C. Huck-Iriart, L. Soler, A. Casanovas, C. Marini, J. Prat, J. Llorca, C. Escudero, Unraveling the Chemical State of Cobalt in Co-Based Catalysts during Ethanol Steam Reforming: an in Situ Study by Near Ambient Pressure XPS and XANES, ACS catal. 8 (10) (2018) 9625–9636, https://doi.org/10.1021/acscatal.8b0266610.1021/acscatal.8b02666.s001.
[28] M. Newville, Fundamentals of XAFS, University of Chicago: Chicago, IL 78 (1) (2014) 33–74, https://doi.org/10.2138/rmg.2014.78.2.
[29] F.W. Lytle, The EXAFS family tree: a personal history of the development of extended X-ray absorption fine structure, J. Synchrotron Radiat 6 (3) (1999) 123–134, https://doi.org/10.1107/S0909049599001260.
[30] D. Koningsberger, B. Mojet, G.V. Dorssen, D. Ramaker, XAFS spectroscopy: Fundamental principles and data analysis, Top. Catal. 10 (2000) 143, https://doi.org/10.1023/A:1019105310221.
[31] A. Moen, D.G. Nicholson, M. Ronning, H. Emerich, *In situ* X-ray absorption spectroscopic studies at the cobalt K-edge on an Al_2O_3-supported rhenium-promoted cobalt Fischer-Tropsch catalyst. Comparing reductions in high and low concentration hydrogen, J. Mater. Chem. 8 (1998) 2533. https://doi.org/10.1039/A804261F.
[32] G. Jacobs, Y. Ji, B.H. Davis, D. Cronauer, A.J. Kropf, C.L. Marshall, Fischer-Tropsch synthesis: Temperature programmed EXAFS/XANES investigation of the influence of support type, cobalt loading, and noble metal promoter addition to the reduction behavior of cobalt oxide particles, Appl. Catal. A: General 333 (2) (2007) 177–191, https://doi.org/10.1016/j.apcata.2007.07.027.
[33] Y. Okamoto, F. Kawamura, Y. Ohta, A.J. Page, S. Irle, K. Morokuma, Self-Consistent-Charge Density-Functional Tight-Binding/MD Simulation of Transition Metal Catalyst Particle Melting and Carbide Formation, J. Comput. Theor. Nanosci. 8 (9) (2011) 1755–1763, https://doi.org/10.1166/jctn.2011.1879.